# Influence of Nanoscale Order-Disorder Transitions on the Magnetic Properties of Heusler Compounds for Spintronics

J. Karel[1]*, J. E. Fischer[1], S. Fabbrici[2], E. Pippel[3], P. Werner[3], M. Vinicius Castergnaro[4], P. Adler[1], S. Ouardi[1], B. Balke[5], G. H. Fecher[1], J. Morais[4], F. Albertini[2], S. S. P. Parkin[3], C. Felser[1]

[1]Max Planck Institute for Chemical Physics of Solids, Dresden, Germany
[2]Institute of Materials for Electronics and Magnetism, Parma, Italy
[3]Max Planck Institute of Microstructure Physics, Halle, Germany
[4]Departamento de Fisica, Instituto de Fisica, Universidade Federal do Rio Grande do Sul (UFRGS), Porto Alegre, RS, Brasil
[5] Institut für Anorganische und Analytische Chemie, Johannes Gutenberg-Universität, Mainz, Germany

*Present address: Department of Materials Science and Engineering, Monash University, Clayton, Victoria, Australia; julie.karel@monash.edu

## Supplementary Information

*Experimental Procedures*

Powder X-Ray diffraction patterns were acquired with an image-plate Huber G670 Guinier camera equipped with a Ge(111) monochromator. To determine the exact lattice parameter additional measurements were carried out using a Si standard reference material (640c). Indexing and refinement of the lattice parameters was done using the programs PowderCell[1] and Win X POW.[2] Scanning electron microscopy (SEM) combined with wavelength-dispersive X-ray spectroscopy (WDS) was used for determining the homogeneity and composition of the compounds.

Hysteresis curves were recorded at 2 K with a superconducting quantum-interference device vibrating sample magnetometer (SQUID-VSM, MPMS 3, Quantum Design)). Thermomagnetic Analysis (TMA)[3] was performed to determine the Curie temperatures of the samples. Temperature dependent AC susceptibility measurements were carried out in an alternating induction field of 0.4 mT with a home-built susceptometer whose working temperature ranges from room temperature to 1373 K.

X-ray absorption spectra at the Co and Fe K-edges were measured on powder samples at XAFS1 beamline of the Brazilian Synchrotron Light Laboratory (LNLS) in Campinas, Brazil. The measurements were performed at room temperature in transmission mode using three $N_2$-filled ionization chambers. X-ray diffraction experiments with synchrotron radiation ($\lambda$ = 1.65307 Å) were performed at bending magnet D10 of the X-ray powder diffraction beamline also at the Brazilian Synchrotron Light Laboratory (LNLS).

TEM images were taken with an FEI TITAN 80-300 transmission electron microscope operated at 300 kV and equipped with a probe corrector for spherical aberrations (Cs corrector). With this high resolution STEM is possible down to atomic dimensions. Image filtering was performed with the Gatan Digital Microscope software.

*Description of Structures*

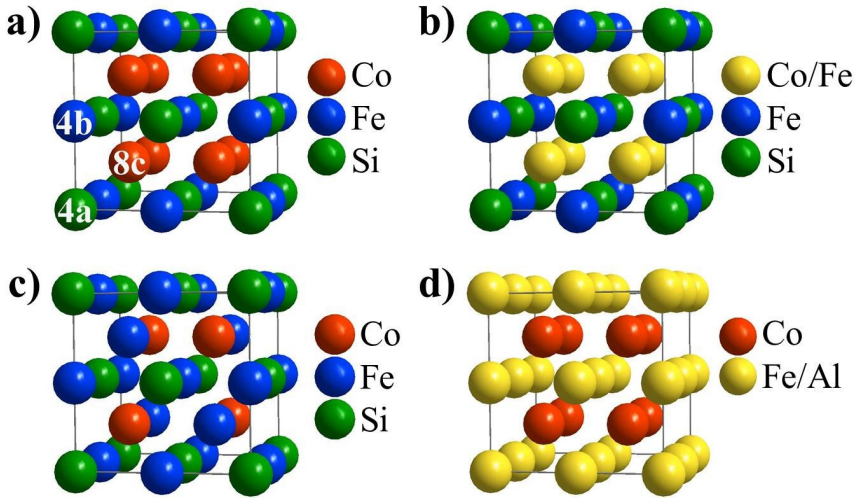


Figure S1. Heusler structures, see text below for description.

**Figure S1** shows **(a)** the regular full-Heusler structure as found for $Co_2FeSi$, space group no. 225, $Fm\bar{3}m$, also designated as $L2_1$, **(b)** the full-Heusler structure with disorder between Co and Fe atoms on the 8c Wyckoff position, occuring in the off-stoichiometric compounds of the $Co_{2-x}Fe_{1+x}Si$ series, **(c)** the inverse Heusler structure, space group no. 216, $F\bar{4}3m$, and **(d)** the CsCl-type structure found for $Co_2FeAl$, space group no. 221, $Pm\bar{3}m$, also named B2. The structures are displayed with multiple unit cells to emphasize the relationship to the inverse full-Heusler compound. The corresponding atoms are labelled with the Wyckoff positions.

*Structural Characterization and Composition*

All x-ray diffraction patterns could be indexed using a face-centered cubic (fcc) space group; the patterns do not show any indication for impurities. For increasing aluminum content, the structure becomes more *B2*-type, which is indicated by a disappearing (111) peak as shown in the inset of figure S2. To quantify the degree of $L2_1$ versus *B2* order, an order parameter ($S$) has been calculated based on the following equation and is listed in Table S1.

$$S = \sqrt{\frac{I_{111}^{exp} / I_{200}^{exp}}{I_{111}^{calc} / I_{200}^{calc}}}$$

$I_{111}^{exp}$ and $I_{200}^{exp}$ are the experimental integrated intensities determined from the (111) and (200) XRD peaks, respectively. $I_{111}^{calc}$ and $I_{200}^{calc}$ are the intensities calculated for the (111) and (200) peaks, respectively, using PowderCell.[1] In addition, a Rietveld refinement performed on the $Co_2FeAl$ XRD pattern indicated a small fraction of the fully chemically disordered A2 structure (90 ± 5% B2 and 10 ± 3% A2). A nearly perfectly linear dependency of the lattice parameter on the composition is found, as shown in the upper right inset of Figure S1 and is clearly visible in the shift of the (220) peak. The lattice constant ranges from $a$ = 5.64 Å for $Co_2FeSi$ to $a$ = 6.70 Å for $Co_2FeAl$, which corresponds to aluminum having a bigger atomic radius.[4]

Figure S3 shows synchrotron X-ray diffraction of the (220) reflection for an $x$=0.2 sample after the normal annealing and quenching procedure and for a sample that underwent the standard annealing and quenching followed by an additional 4 annealing cycles (as described in the main text). After the additional annealing cycles (red curve), the peak does not present any asymmetry, indication of an impurity phase or change in lattice constant. The peak is slightly broadened, likely resulting from the increased disorder induced during the annealing.

SEM/WDS analysis revealed average sample compositions consistent with the targeted values (Table S2). Compositional fluctuations of up to ±3 at% were observed on the length scale of ~20μm in all off-stoichiometry samples. For $x$=0.4, the variation was ±5 at%. However, the variations in chemical order were observed on the nm length scale, meaning within a single composition. Therefore, we do not believe slight compositional variations contributed to the observed experimental results.

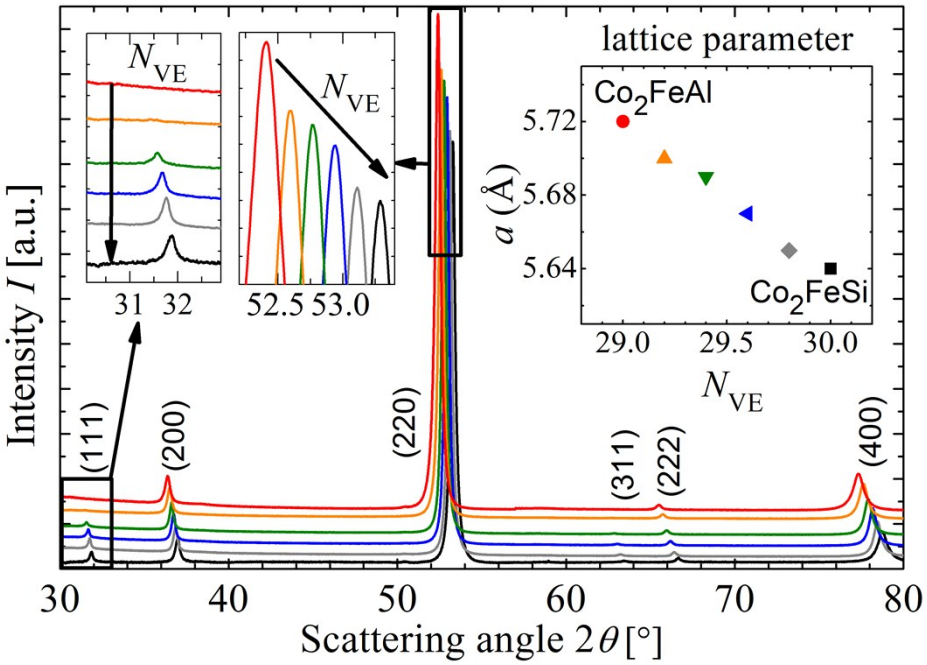


**Figure S2.** Powder X-ray diffraction patterns of the $Co_2FeSi_xAl_{1-x}$–series. The insets on the left show magnifications of the patterns and in the upper right corner the lattice parameter is given as a function of the composition.

| **Composition** | ***S*** |
|---|---|
| $Co_2FeSi$ | 0.5 |
| $Co_2FeSi_{0.8}Al_{0.2}$ | 0.47 |
| $Co_2FeSi_{0.6}Al_{0.4}$ | 0.42 |
| $Co_2FeSi_{0.4}Al_{0.6}$ | 0.33 |
| $Co_2FeSi_{0.2}Al_{0.8}$ | 0 |
| $Co_2FeAl$ | 0 |

**Table S1.** Calculated order parameter, $S$, for the compositions investigated in this work.

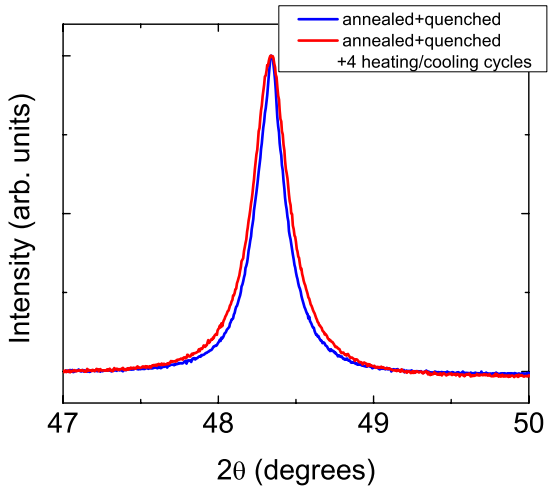


**Figure S3.** X-ray diffraction of the (220) reflection of $x$=0.2 sample as-prepared (blue) and after 4 annealing cycles (red) measured with synchrotron radiation (λ = 1.65307 Å).

| **Compound** | **Target Composition** [at%] | | | | **Experimental Composition** [at%] | | | | | | | | ***a*** [Å] |
|---|---|---|---|---|---|---|---|---|---|---|---|---|---|
| | Co | Fe | Al | Si | Co | dev Co | Fe | dev Fe | Al | dev Al | Si | dev Si | |
| $Co_2FeAl$ | 50 | 25 | 25 | 0 | 49.5 | 0.5 | 26.3 | 2.9 | 24.2 | 2.5 | - | - | 5.72 |
| $Co_2FeAl_{0.8}Si_{0.2}$ | 50 | 25 | 20 | 5 | 49.1 | 0.2 | 24.6 | 2.1 | 21.1 | 3.1 | 5.2 | 1.0 | 5.70 |
| $Co_2FeAl_{0.6}Si_{0.4}$ | 50 | 25 | 15 | 10 | 49.2 | 0.1 | 24.6 | 1.3 | 16.6 | 2.5 | 9.6 | 1.2 | 5.69 |
| $Co_2FeAl_{0.4}Si_{0.6}$ | 50 | 25 | 10 | 15 | 49.3 | 0.1 | 24.6 | 1.5 | 11.5 | 3.6 | 14.6 | 2.1 | 5.67 |
| $Co_2FeAl_{0.2}Si_{0.8}$ | 50 | 25 | 5 | 20 | 49.6 | 0.2 | 25.2 | 0.5 | 19.7 | 0.8 | 5.6 | 1.1 | 5.65 |
| $Co_2FeSi$ | 50 | 25 | 0 | 25 | 49.9 | 0.1 | 25.2 | 0.1 | . | . | 49.9 | 0.0 | 5.64 |

**Table S2.** Average composition and lattice constants for samples investigated

*Mössbauer Spectroscopy*

$^{57}$Fe Mössbauer spectra of the $Co_2FeSi_xAl_{1-x}$–series (Fig. S4) were collected at room temperature and evaluated as described elsewhere.[5] All the spectra consisted of a single, somewhat broadened magnetic hyperfine sextet that was fitted by a hyperfine field distribution model. The resulting isomer shifts *IS* and peak hyperfine fields $B_{hf}$ are depicted in Fig. S5. The $B_{hf}$ values (> 30 T) confirm that all the Fe atoms reside on the *4a* or *4b* sites of the Heusler structure. There are no indications for Fe-Co disorder which would result in a second hyperfine component with $B_{hf}$ ~ 20 T. The *B*2-type disorder is reflected in a subtle modification in the shape of the hyperfine field distribution. In particular, the distributions are broader for members with mixed Si/Al contents and for $Co_2FeAl$ compared to $Co_2FeSi$. However, the gross $B_{hf}$ is not affected by the disorder as the nearest neighbor environment of Fe (8 Co atoms) remains unchanged. The change in composition is reflected in a modification of the *IS* and $B_{hf}$ values across the series (Fig. S5), in agreement with a previous report.[6] Most remarkably, the change in *IS* upon going from $Co_2FeAl$ to $Co_2FeSi$ in the series $Co_2FeSi_xAl_{1-x}$ ($\Delta N_{VE}$ = 1, $\Delta IS$ = 0.11

mm $s^{-1}$) is considerably more pronounced than in the corresponding $Co_{2-x}Fe_{1+x}Si$ series ($\Delta N_{VE}$ = 1, $\Delta IS$ = 0.03 mm $s^{-1}$) .[5]

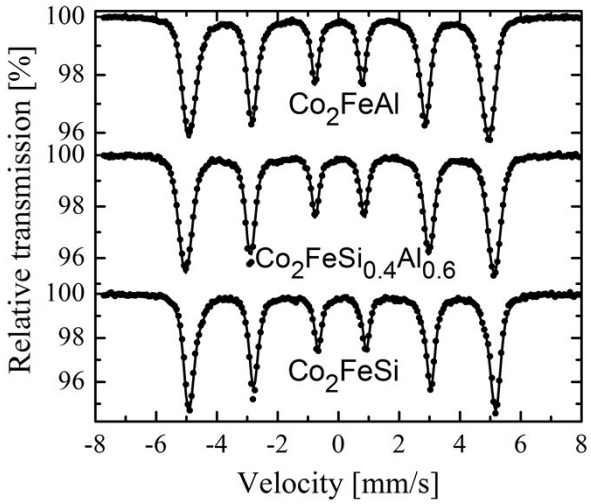


**Figure S4.** Mössbauer spectra of three samples from the $Co_2FeSi_xAl_{1-x}$ series at room temperature. The black dots are the experimental data, and the solid lines are the fits that were carried out using only one magnetic component.

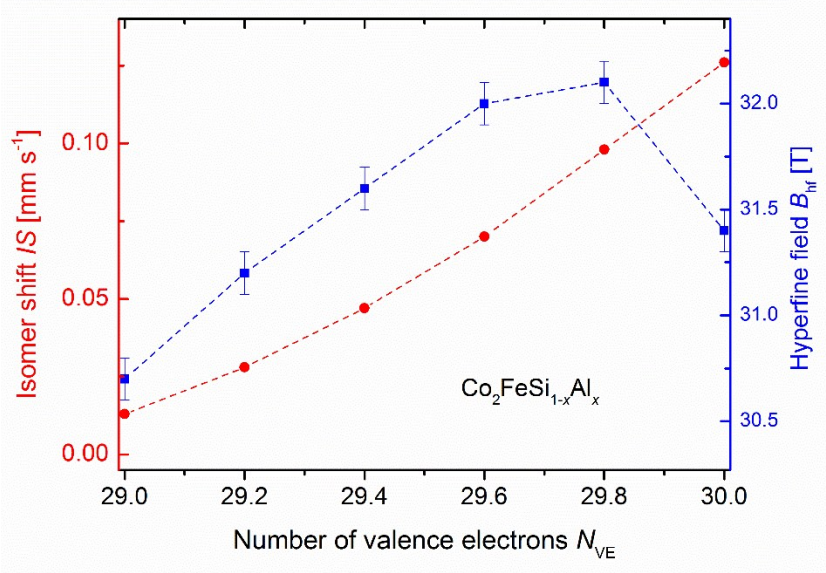


**Figure S5.** Isomer shifts *IS* and magnetic hyperfine fields $B_{hf}$ of the $Co_2FeSi_xAl_{1-x}$ series. Solid lines are guides-to-the eye.

*X-ray Absorption Fine Structure*

X-ray absorption data at the Co and Fe K-edges were measured on powders made from the samples at XAFS1 beamline of the Brazilian Synchrotron Light Laboratory (LNLS). The measurements were performed at room temperature in transmission mode using three $N_2$-filled ionization chambers. The $L2_1$ and *B2* structures present different signatures in the EXAFS signals at the Fe K edge because Fe atoms have a different chemical environment in each case. For instance, assuming $Co_2FeZ$ (Z = Al, Si) in a perfect *B2* structure, the absorbing Fe atoms have 8 Co atoms in the coordination shell (CS). The second nearest neighbors consist of 3 Z

atoms and 3 Fe atoms, followed by 6 Z atoms and 6 Fe atoms as the third nearest neighbors. On the other hand, a perfect $Co_2FeZ$ $L2_1$ structure has the Fe atoms surrounded by 8 Co atoms in the CS, 6 Z atoms and 12 Fe atoms as second and third nearest neighbours, respectively. These clear differences in the short range order around Fe lead to distinct photoelectron scattering processes within the sample and, thus, to distinct EXAFS signals. FEFF 9.6[7] code was used to calculate the scattering amplitudes and phase shifts resulting from the photoelectron scattering processes in both *B2* and $L2_1$ structures for $Co_2FeZ$. The output of each calculation was used to adjust the FTs of samples #1 and #2 (both $Co_2FeSi_{0.2}Al_{0.8}$ with different heat treatments, as discussed in the main text). For both samples, the fitting quality was higher when the *B2* structure was used (the R-factors using *B2* structure were about two orders lower than for $L2_1$), which means that *B2* is the preferred structure for this composition. Tables S3 and S4 show the structural parameters determined from the fits to the EXAFS data for the Fe and Co K edges respectively, and figure S6 displays the EXAFS oscillations extracted from the EXAFS data for both K edges.

| Sample | Pair | N | R (Å) | $\sigma^2$ ($10^{-2}$ Å$^2$ ) |
|---|---|---|---|---|
| Sample #1 | **Fe-Co** | 8.0 ± 0.1 | 2.46 ± 0.02 | 0.40 ± 0.02 |
| | **Fe-Z** | 3.6 ± 0.2 | 2.84 ± 0.02 | 0.64 ± 0.05 |
| | **Fe-Fe** | 2.5 ± 0.2 | 2.85 ± 0.02 | 0.62 ± 0.04 |
| | **Fe-Z** | 5.6 ± 0.1 | 4.01 ± 0.02 | 0.82 ± 0.03 |
| | **Fe-Fe** | 6.6 ± 0.2 | 4.01 ± 0.02 | 0.83 ± 0.08 |
| | **Fe-Co** | 24.0 ± 0.1 | 4.72 ± 0.02 | 0.97 ± 0.02 |
| | **Fe-Z** | 4.0 ± 0.2 | 4.94 ± 0.02 | 0.98 ± 0.01 |
| | **Fe-Fe** | 3.9 ± 0.2 | 4.95 ± 0.02 | 0.93 ± 0.02 |
| Sample #2 | **Fe-Co** | 8.0 ± 0.1 | 2.46 ± 0.02 | 0.44 ± 0.03 |
| | **Fe-Z** | 3.1 ± 0.1 | 2.84 ± 0.02 | 0.68 ± 0.03 |
| | **Fe-Fe** | 2.8 ± 0.2 | 2.85 ± 0.02 | 0.69 ± 0.04 |
| | **Fe-Z** | 5.8 ± 0.1 | 4.01 ± 0.02 | 0.91 ± 0.03 |
| | **Fe-Fe** | 6.3 ± 0.1 | 4.01 ± 0.02 | 0.95 ± 0.05 |
| | **Fe-Co** | 24.0 ± 0.2 | 4.72 ± 0.02 | 0.95 ± 0.02 |
| | **Fe-Z** | 4.0 ± 0.2 | 4.94 ± 0.02 | 0.98 ± 0.03 |
| | **Fe-Fe** | 4.0 ± 0.2 | 4.95 ± 0.02 | 0.97 ± 0.04 |

**Table S3**. Structural parameters obtained from Fe K edge EXAFS analysis. Both samples are $Co_2FeSi_{0.2}Al_{0.8}$, with different heat treatments as discussed in the main text.

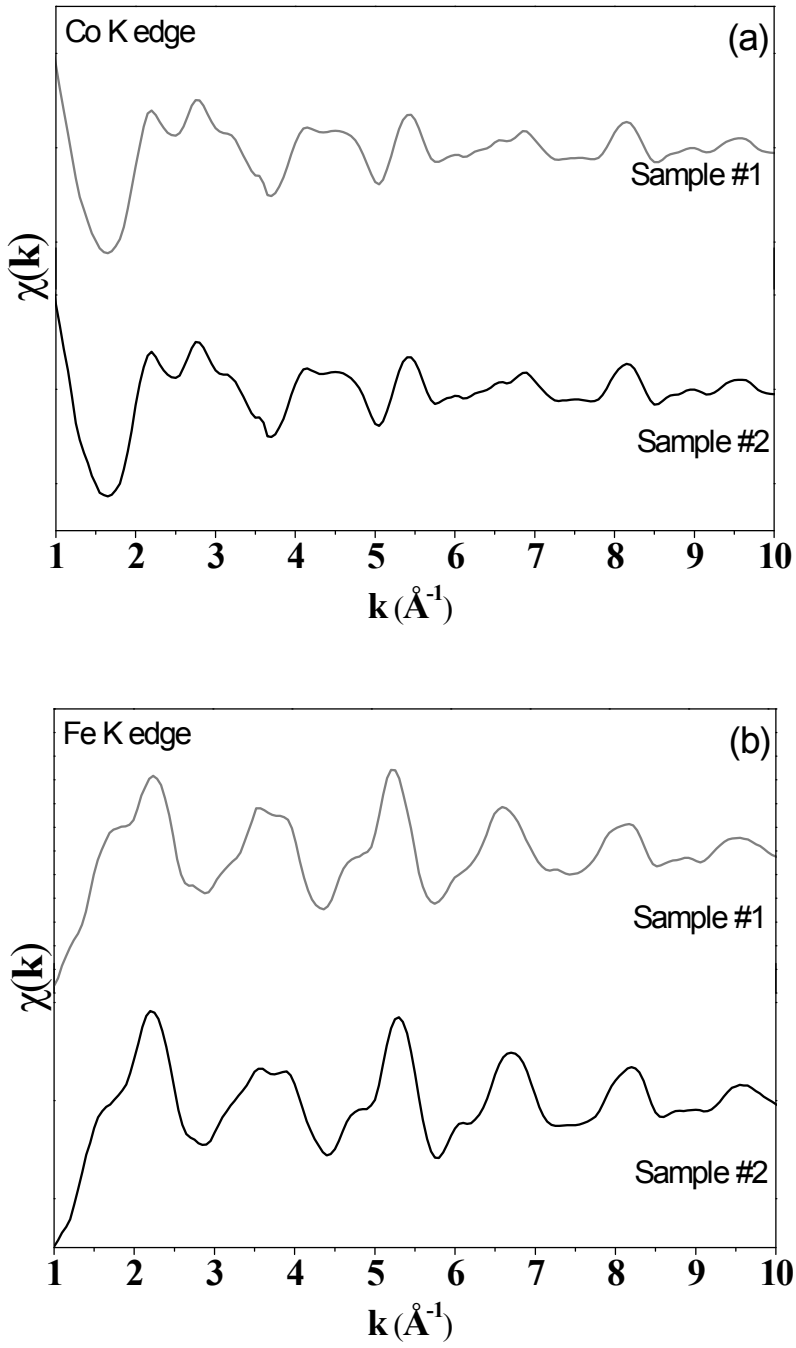


**Figure S6.** EXAFS oscillations extracted from the XAFS data at the Co (a) and Fe (b) K edges of sample #1 (grey lines) and sample #2 (black lines).

| Sample | Pair | N | R (Å) | $\sigma^2$ ($10^{-2}$ Å$^2$ ) |
|---|---|---|---|---|
| Sample #1 | **Co-Fe** | 4.0 ± 0.2 | 2.47 ± 0.02 | 0.50 ± 0.04 |
| | **Co-Z** | 4.0 ± 0.2 | 2.47 ± 0.02 | 0.55 ± 0.04 |
| | **Co-Co** | 6.1 ± 0.1 | 2.86 ± 0.02 | 0.63 ± 0.04 |
| | **Co-Co** | 12.0 ± 0.1 | 4.01 ± 0.02 | 0.78 ± 0.07 |
| | **Co-Fe** | 12.0 ± 0.2 | 4.73 ± 0.02 | 0.91 ± 0.02 |
| | **Co-Z** | 12.0 ± 0.1 | 4.73 ± 0.03 | 0.93 ± 0.02 |
| | **Co-Co** | 8.1 ± 0.1 | 4.96 ± 0.02 | 0.89 ± 0.03 |
| Sample #2 | **Co-Fe** | 4.0 ± 0.1 | 2.47 ± 0.02 | 0.52 ± 0.02 |
| | **Co-Z** | 4.0 ± 0.1 | 2.48 ± 0.02 | 0.56 ± 0.03 |
| | **Co-Co** | 6.0 ± 0.1 | 2.85 ± 0.02 | 0.63 ± 0.07 |
| | **Co-Co** | 12.1 ± 0.1 | 4.02 ± 0.02 | 0.82 ± 0.05 |
| | **Co-Fe** | 12.0 ± 0.2 | 4.73 ± 0.02 | 0.92 ± 0.01 |
| | **Co-Z** | 12.0 ± 0.1 | 4.72 ± 0.03 | 0.95 ± 0.03 |
| | **Co-Co** | 8.0 ± 0.1 | 4.96 ± 0.02 | 0.99 ± 0.06 |

**Table S4**. Structural parameters obtained from Co K edge EXAFS analysis. Both samples are $Co_2FeSi_{0.2}Al_{0.8}$, with different heat treatments as discussed in the main text.

*Magnetic Properties*

Figure S7 shows the magnetic hysteresis loops acquired at 2 K. The materials are soft ferromagnets, and the magnetic moment shown in Figure 1a was determined from the saturation value of these hysteresis curves.

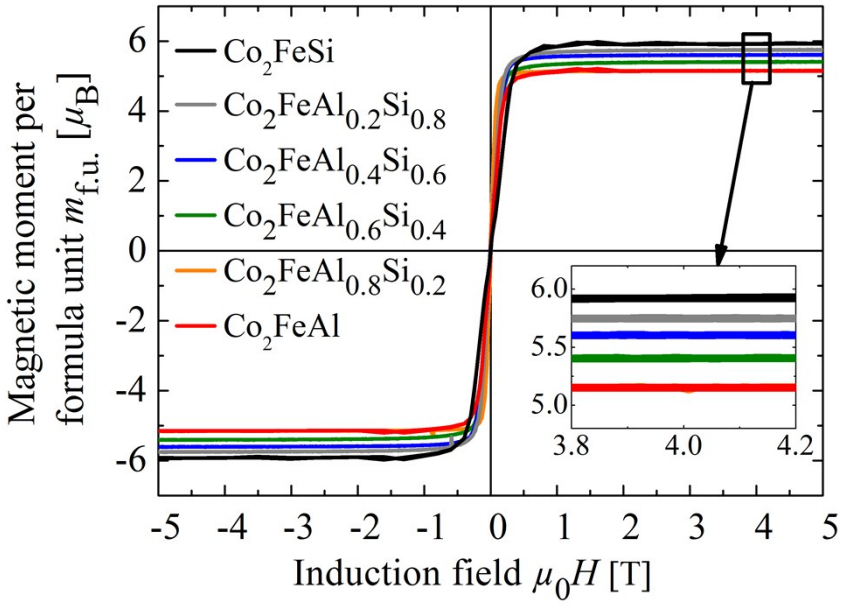


**Figure S7.** Hysteresis curves of all samples detected at a temperature of 2 K. The magnetic moment in saturation increases continuously with increasing Si content.

During several heating and cooling cycles in the TMA apparatus, the second, higher transition temperatures changes slightly to higher and lower values until reaching an equilibrium state in which the transition temperature and the transition's intensity remain stable. The values shown for the $T_C$ in table 1 and Figure 1a are determined from the equilibrium signal. Thermomagnetic analysis reveals a linear trend of the $T_C$ (Figure 1b) with composition. The magnetization does not follow a Brillouin function, thus the inflection point of the curve was used as the Curie temperature. This value is less dependent on the broadness of the signal, which can vary with the applied magnetic field or homogeneity of the sample. The transition temperature found for $Co_2FeSi$ is 1045 K with an uncertainty of 0.24 %. This value is in very good agreement with the inflection point determined from the measurements carried out by Wurmehl *et al.*[8] For $Co_2FeAl$ the transition temperature is 1218 K, which is a record value for a Curie temperature in Heusler compounds.

**Supplementary Information References**

[1] PowderCell for Windows Version 2.4, Federal Institute for Materials Research and Testing, Berlin, Germany, (2009)
[2] STOE WinXPOW Version 2.25, Stoe & Cie GmbH, Darmstadt, Germany, **2009**
[3] R. Grössinger, G. Hilscher, H. Kirchmayr, *Mikrochim. Acta* **1981**, *9*, 161
[4] J. C. Slater, *J. Chem. Phys.* **1964**, *41*, 3199
[5] J.E. Fischer, J. Karel, S. Fabbrici, P. Adler, S. Ouardi, G. H. Fecher, F. Albertini, C. Felser, *Phys. Rev. B*, **94** 024418 (2016)
[6] L. F. Kiss, G. Bortel, L. Bujdosó, D. Kaptás, T. Kemény, I. Vincze, *Acta Phys. Pol. A* **127,** 347 (2015)
[7] J.J. Rehr, J.J. Kas, F.D. Vila, M.P. Prange, K. Jorissen, *Phys. Chem. Chem. Phys.* **12** 5503 (2010)
[8] S. Wurmehl, G. H. Fecher, V. Ksenofontov, F. Casper, U. Stumm, C. Felser, H. Lin, Y. Hwu, *J. Appl. Phys.* **99** 08J103 (2006)